J Electroceram (2018) 40:79–87
DOI 10.1007/s10832-017-0105-y

CrossMark

Characterization of RF sputtered zinc oxide thin films on silicon using scanning acoustic microscopy

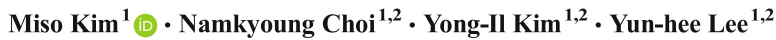
Miso Kim [1] · Namkyoung Choi [1,2] · Yong-Il Kim [1,2] · Yun-hee Lee [1,2]

Received: 3 August 2016 / Accepted: 25 September 2017 / Published online: 15 October 2017
© Springer Science+Business Media, LLC 2017

Abstract Zinc oxide (ZnO) thin films were grown on silicon (100) substrate using radio frequency (RF) sputtering under various processing parameters including deposition time and annealing temperature. A series of characterization techniques including X-ray diffraction (XRD), scanning electron microscopy (SEM), atomic force microscopy (AFM) and scanning acoustic microscopy (SAM) have been used to analyze the crystallinity and crystal orientation, structural morphology, surface roughness, and acoustic properties of these films. In particular, quantitative analysis of elastic wave propagation in ZnO thin films by scanning acoustic microscopy has been performed for the first time in the present work. It has been shown that the propagation properties of acoustic waves on the surface of ZnO thin films strongly depend on film thickness, crystallinity, and surface roughness. The dispersion properties of surface acoustic waves (SAWs) are observed as a function of ZnO film thickness. The velocities of SAWs range from 5328.3 m/s to 4245.7 m/s with increasing film thickness from 32.5 nm to 2.04 μm, while smoother surface contributes to faster propagation of SAWs.

Keywords ZnO thin films · Scanning acoustic microscopy · Surface acoustic waves · RF sputtering

✉ Miso Kim
misokim@kriss.re.kr

[1] Korea Research Institute of Standards and Science, Daejeon, Republic of Korea

[2] Korea University of Science and Technology, Daejeon, Republic of Korea

1 Introduction

Zinc oxide (ZnO) is a material that possesses both piezoelectric and semiconducting properties, thus attracting widespread international interest. Use of such properties has led to emerging applications of ZnO thin films for thin films transistors, transparent electrodes, energy harvesting and surface acoustic wave (SAW) devices. Radio frequency (RF) sputtering technique is one of the most common methods to deposit ZnO thin films and there have been a number of studies on the piezoelectric, optical, electronic, structural and mechanical properties of RF sputtered ZnO thin films as a function of processing parameters [1–8]. Understanding the correlation of material properties with processing conditions is considerably important because it enables systematic design and fabrication of ZnO thin films suitable for the target applications of interest.

Acoustic microscopy is a powerful nondestructive technique for materials characterization where acoustic waves are used as probes as a counterpart to the light in optical microscopy. Incident acoustic waves penetrate through solids and interact with the elastic properties of materials. Analysis of the reflected signal of acoustic waves provides useful means not only to observe internal and subsurface structures of even optically opaque specimens but also to determine acoustic characteristics of materials (Fig. 1). The principle of operation, resolution, penetration ability, and contrast mechanisms of acoustic microscopy are thoroughly reviewed in a prior publication by Yu and Boseck [9]. Here, two operating modes – imaging and materials characterization – are briefly described to help understanding of the work done in this paper.

In the imaging mode, any change in substructure such as discontinuities and elastic properties will result in signal changes during scanning, which in turn are used to generate a contrast image of the interference. Thus, acoustic

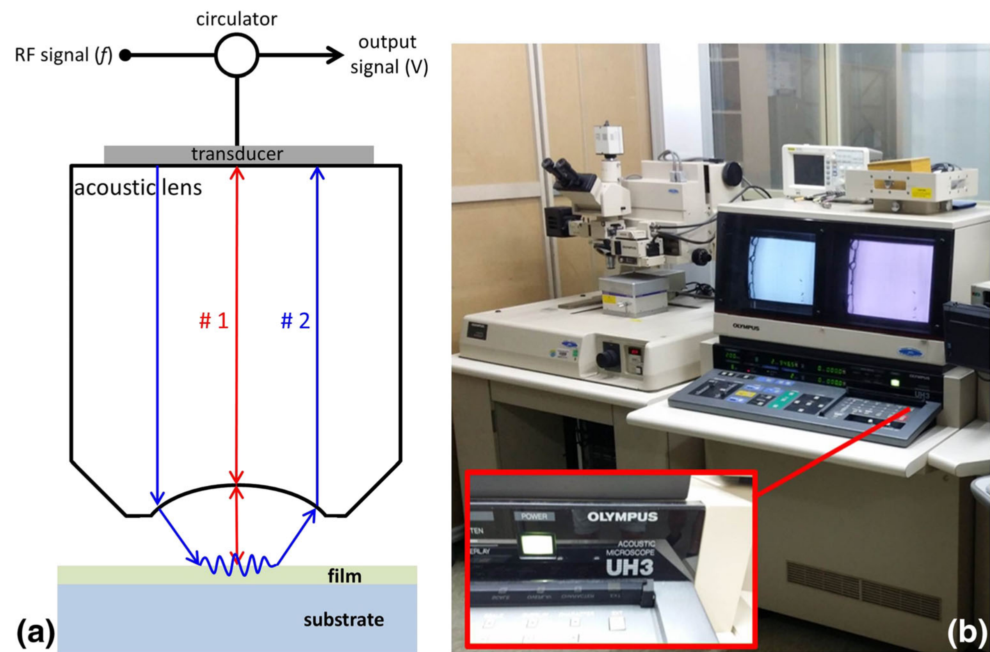

Fig. 1 (**a**) Schematic of the operation principle in acoustic microscopy and (**b**) scanning acoustic microscope used in this work (Olympus, UH-3)

micrographs have been usefully utilized to "see" the internal structures and subsurface defects [10, 11].

Acoustic microscopy also offers quantitative evaluation of surface elastic properties of materials. This materials characterization technique is related to *V*(*z*) curve, also known as acoustic materials signature (AMS) [12, 13]. When acoustic beams are focused on the specimen surface through the acoustic lens, surface acoustic waves (SAWs) propagate along the interface of a material and water and then radiate into the liquid. Interference of this reflected leaky surface acoustic waves (LSAWs) (track #2 in Fig. 1(a)) and the waves specularly reflected from the incident waves (track #1 in Fig. 1(a)) generates periodic oscillations of transducer voltage output, *V* as a function of the distance *z* between the focal point of acoustic lens and the specimen surface [14]. Since the spacing of peaks or periodicity of the *V*(*z*) curve is directly related to the surface acoustic wave velocity of the material investigated, it is possible to calculate the SAW velocity from the V(z) curve measurement. The shapes of *V*(*z*) curves are uniquely dependent on the materials interested. Accordingly, *V*(*z*) measurement allows quantitative analysis of surface elastic properties of the specimen material [15, 16].

Evaluation of SAW velocity from the *V*(*z*) measurement provides a useful diagnostic tool for material characterization particularly of thin film structures. The propagation behavior of surface acoustic waves in layered structures is different from that of bulk solids. In a layered structure like a thin film deposited on a substrate, surface acoustic waves become dispersive in that SAW velocity depends on frequency of excitation, layer thickness, and elastic parameters [9]. In a thin film structure, the energy from the transmitted wave has a penetration depth approximately equal to one wavelength [17]. Because of the energy distribution between film and substrate, SAW velocity variation occurs as a function of the thin film thickness and wavelength. In other words, changes in film thickness as well as frequency result in a dispersive characteristic of SAW velocities. Therefore, examination of dispersion properties of SAWs in a thin film structure enables estimation of film thickness and determination of elastic properties. Weglein demonstrated a pioneering work on the application of acoustic microscopy to SAW dispersion and film thickness measurement in 1979 and 1980 [13, 18]. Using the SAW velocity data measured by acoustic microscopy, he derived the thicknesses of gold films deposited on a < 100> silicon wafer [13]. Theoretical modeling was also followed. Kundu et al. developed an analytical model of the acoustic materials signature for multilayered structures, which was applied to the calculation of AMS of the copper coated fused quartz substrate with coating thickness of 2 μm [19].

Acoustic microscopy has also been used for quantitative measurement of elastic properties of thin films. Achenbach et al. estimated the elastic constants of anisotropic thin films consisting of TiN and VN films deposited on (001) MgO substrates from V(z) measurements obtained by using line focus acoustic microscopy [20, 21]. Robert et al. obtained and compared elastic properties of TiN coating and C-Cr coating on a steel substrate by using different techniques including impact excitation, indentation, and V(z) measurement of acoustic microscopy [17]. Later, Bamber et al. demonstrated the potential for combining nanoindentation and V(z) acoustic microscopy to determine an unknown Young's modulus and Poisson's ratio of thin films [22]. Benbelghit et al. proposed a

semi-empiric approach to estimation of elastic properties of one layer coated materials (e.g., Cr on Fe, TiN on Fe, Al on Si, and Al on SiC) [23].

In the present work, quantitative analysis of elastic wave propagation in ZnO thin films deposited on silicon (001) substrate has been performed by scanning acoustic microscopy for the first time. SAW velocities of ZnO thin films deposited under various sputtering conditions are determined from the $V(z)$ measurement. Fabrication of SAW devices with complex electrode structures is normally required to determine the SAW velocities. In contrast, scanning acoustic microscopy offers a nondestructive materials characterization method for as-deposited thin films without a need for device fabrication. The correlation of surface elastic properties of ZnO thin films with thin film growth is thoroughly studied through X-ray diffraction (XRD), atomic force microscopy (AFM), scanning electron microscopy (SEM) and scanning acoustic microscopy (SAM) techniques. Structural and acoustic characterization in this work would provide useful information on the magnitude and trend of SAW velocities in ZnO thin films as a function of RF sputtering conditions, which can be considered in device design of SAW sensor or ultrasonic transducer applications.

2 Experimental details

ZnO films were deposited on Si substrates using RF magnetron sputtering from a ZnO target (99.9%). Substrate is n-type silicon with (100) orientation and the resistivity is 1–10 Ω-cm. The RF power, gas pressure, and substrate temperature were set at 200 W, 5 mTorr, and room temperature (24 °C) as listed in Table 1. The target was pre-sputtered before the actual deposition to prevent any contamination of the target surface. In order to study the influence of processing conditions, deposition time and annealing temperature were set as variable parameters. First, we fabricated films with various deposition times of 30 min, 1, 2, 3, 5, 6, 7, to 10 h and all deposited films were annealed at 600 °C for 50 min. In the second set of experiment, eight samples of ZnO films were deposited for 6 h and then annealed. Each of seven samples was annealed at different temperature (100, 200, 300, 400, 500, 550, and 600 °C) for 50 min while one sample remained as-deposited. Annealing process was conducted under O_2 environment (20 sccm).

Table 1 Sputtering conditions for deposition of ZnO thin films used in this work

Target composition	ZnO target
Target-substrate distance [mm]	70
Substrate temperatures [°C]	Room temperature (24 °C)
RF power [W]	200
Sputtering gas	Ar (60 sccm), no O_2 gas
Deposition pressure [mTorr]	5
Deposition time [hours]	0.5, 1, 2, 3, 5, 6, 7, 10
Annealing temperature [°C]	100, 200, 300, 400, 500, 550, 600
Annealing time [min.]	50
Annealing environment	O_2 gas (20 sccm)

The correlation among processing conditions, physical structures and acoustic properties of the films were investigated by various techniques. The crystallinity and crystal orientation of the films were characterized by X-ray diffraction (XRD). XRD data were collected over the scattering angle range $5° \leq 2\theta \leq 100°$ at a 2θ step of 0.02° using CuK_α radiations with a graphite monochromator in the reflection geometry at room temperature (Rigaku, Dmax 2200 V). For further investigation of the crystal qualities, the values of full width at half maximum (FWHM) of different sputtering ZnO thin films were obtained by spanning the XRD diffraction angles (2θ) from 33.5°to 35.5°. Scanning electron microscopy (SEM) was used to determine the thickness and study the microstructure of the ZnO film layers. The topographic characterizations including surface morphology and roughness were conducted by atomic force microscopy (AFM, Park Systems-XE 100). The AFM data were collected using silicon cantilevers from the surface area of 5 μm × 5 μm in contact mode.

Scanning acoustic microscope (Olympus, UH-3) with a point focused transducer was used in the reflection mode to perform $V(z)$ measurement (Fig. 1(b)). The same measurement system has been described in detail in [24]. For an acoustic lens, we employed AL4M631, which is a burst acoustic lens with an aperture angle of 120° and a center frequency of 400 MHz. The phase velocities of leaky surface acoustic waves (or leaky Rayleigh waves) are determined from the interval Δz in the $V(z)$ curve. Eq. (1) allows calculation of the LSAW velocity from the $V(z)$ curve [10]:

$$v_{LSAW} = \frac{v_0}{\left\{1-\left(1-\frac{v_0}{2f\Delta z}\right)^2\right\}^{1/2}} \tag{1}$$

where v_0 is the velocity of acoustic waves in the coupling fluid and f is the frequency. Distilled water was used as a coupling fluid at room temperature. In the present work, the velocity of the acoustic wave in distilled water was assumed to be 1505.9 m/s. Detailed procedure was as follows: Fast Fourier Transform (FFT) waveform analysis was applied to determine the frequency spectra of interest from the measured $V(z)$ curve. We then applied digital filtering technique to the frequency spectra to remove background and noise during the measurement. Inverse Fast Fourier Transform (IFFT) was conducted to gain the digitally filtered $V(z)$ curve. The value of LSAW velocity was finally obtained by applying FFT technique to the digitally filtered $V(z)$ curves.

3 Results and discussion

Thickness of the deposited ZnO films is determined via the cross-section SEM imaging. Figure 2 shows that the thickness of ZnO films increases from 32.5 ± 2.5 nm to 2.04 ± 0.02 μm when deposition time increases from 30 min to 10 h. The average deposition rate is found to be about 3.35 nm/min, leading to an almost linear increase in the film thickness. As will be shown in Fig. 10, all the thicknesses of the ZnO films deposited for 6 h and annealed at eight different annealing temperatures (i.e., 100, 200, 300, 400, 500, 550, 600 °C) are observed to be around 1.01 μm ± 0.09 μm. Therefore, it can be concluded that deposition time is one of the dominant processing parameters in controlling film thickness while annealing temperature seems to have little influence on film thickness.

Figure 3 shows X-ray diffraction (XRD) patterns of the deposited ZnO films as a function of deposition time. All the XRD spectra of ZnO films deposited under various sputtering conditions exhibit a single characteristic peak at around $2\theta = 34.4°$, which corresponds to the diffraction from the (002) plane of the hexagonal wurtzite structure. This confirms fabrication of highly c-axis textured ZnO films. As indicated in Fig. 3 and Table 2, the 2θ diffraction angle slightly shifts from 34.5° to 34.4°, when the deposition time increases from 30 min to 10 h. This implies increase in the *a*-axis and *c*-axis lattice parameters, which will be discussed further in the following paragraph. With increasing deposition time, the intensity of the peaks increases accordingly. This result seems closely related to the thickness of the deposited films. Longer deposition time results in thicker films, which leads to the stronger intensity of the diffracted peaks at around $2\theta = 34.4°$.

In Table 2, the lattice parameters of *a*-axis and *c*-axis are presented as a function of deposition time. In order to refine lattice parameters of the ZnO thin films, a position-constrained pattern decomposition called Pawley refinement, in which the unit cell, zero point and peak profile parameters are varied in a least-squares fit to the diffraction data, was used [26]. The zero-point shift associated with the alignment of the diffractometer was corrected with X-ray powder diffraction data of a standard reference material (SRM) 640c (NIST) to account for the peak shifts in the diffraction patterns recorded. Initial crystal structural information of ZnO is a hexagonal crystal system with space group of P 63 m c [27, 28]. With increasing deposition time, both *a*-axis and *c*-axis lattice parameters are found to increase and approach those of bulk ZnO [29]. It should be noted that various lattice parameters of bulk ZnO are available in the open literature (a = 3.2500 ~ 3.2648 Å and c = 5.2040 ~ 5.2194 Å, respectively) [25, 30–32], while we indicated one representative values in Table 2. Possible reason for this might be the compressive residual stress between Si substrate and ZnO film [33]. Thin films are subject to compressive residual stress generated due to the substrate when films are relatively thin. As films become thicker with increasing deposition time, the influence from the substrate becomes weaker. Accordingly, relaxation of compressive residual stress occurs, which leads to the increase in lattice parameters. Relaxation of compressive residual stress is also

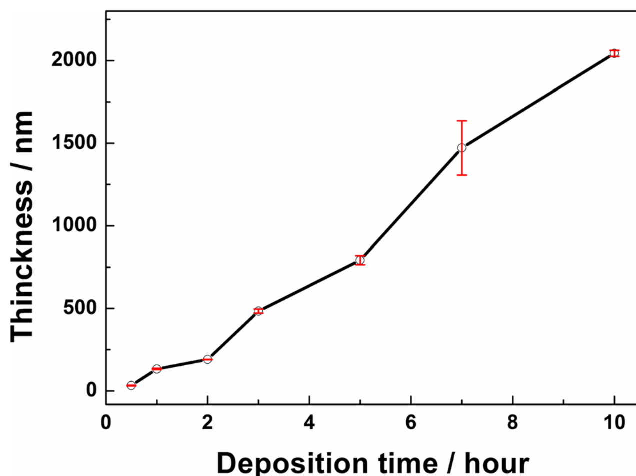

Fig. 2 ZnO film thickness as a function of deposition time

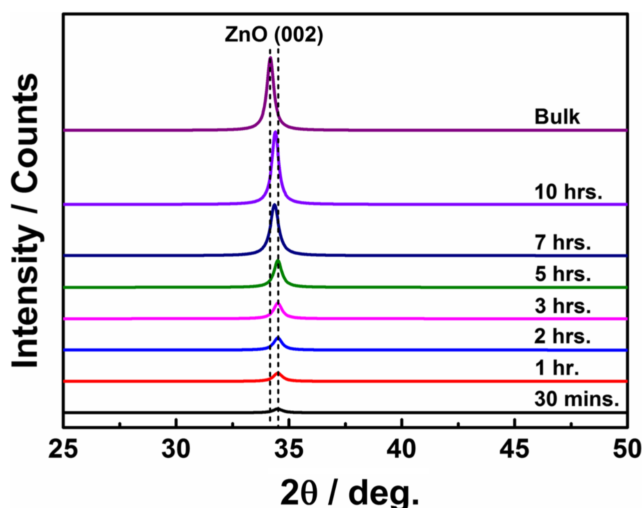

Fig. 3 XRD patterns of the deposited ZnO films as a function of deposition time

Table 2 Variation of 2θ diffraction angles and lattice parameters depending on deposition time

Time (hrs.)	2θ (°)	*a*-axis (Å)	*c*-axis (Å)
0.5	34.5	3.2223	5.1944
1	34.5	3.2216	5.1951
3	34.5	3.2286	5.1963
5	34.5	3.2288	5.1984
7	34.4	3.2300	5.2159
10	34.4	3.2441	5.2175
bulk [25]	34.2	3.2500	5.2040

related to the dispersive behavior of ZnO thin films, which will be addressed later.

From the profile analysis of (002) reflection, FWHM is obtained as a function of film thickness that corresponds to the deposition time. FWHM decreases from 0.37° to 0.25° when the film thickness increases from 32.5 nm to 2.04 μm. This suggests that slightly higher crystallinity is observed when films become thicker. According to Scherrer's equation, crystallite size, which is inversely proportional to FWHM, was calculated and plotted in Fig. 4(a) [34, 35]. With increasing deposition time, crystallite size is found to increase from 22.2 to 30.6 nm, as seen in Fig. 4(a). Figure 4(b) contains the result of the calculated crystallite sizes as a function of annealing temperature. The values of FWHM range from 0.24° to 0.27°. The average crystallite size in Fig. 4(b) is about 32.4 nm with a minimum value of 30.5 nm and maximum value of 34.3 nm. Both FWHM and crystallite size do not exhibit pronounced tendency depending on the annealing temperature, when compared to deposition time.

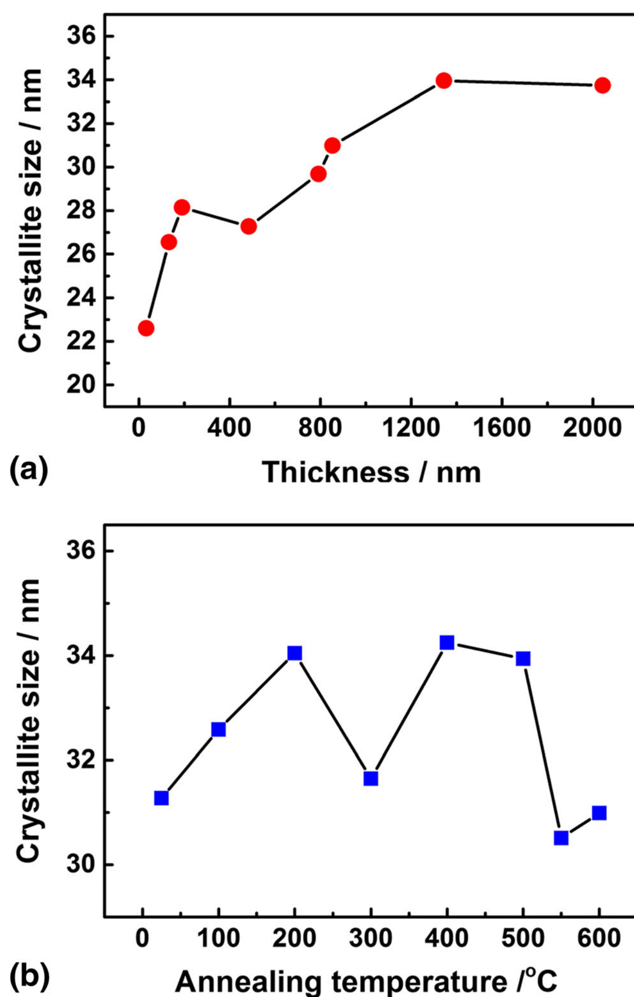

Fig. 4 Crystallite sizes as a function of (**a**) deposition time and (**b**) annealing temperature

SEM characterization was performed to study the layer microstructure and surface morphology. Evolution of film morphology towards columnar grain structures is observed as deposition time increases. The columnar structures become more prominently seen in ZnO films deposited for more than 5 h, as shown in Fig. 5 where cross-sectional views of the ZnO thin films deposited for 7 and 10 h, respectively, are presented. The columnar structures are proved to have a parallel *c*-axis (002) orientation as ZnO crystals typically grow as long hexagonal rods along *c*-axis [7]. Observation of more noticeable grain growth towards columnar structures with increasing deposition time suggests that longer deposition time causes films to have stronger *c*-axis (002) orientation. This result is consistent with that of the XRD patterns in Fig. 3 where peak intensities at (002) reflection increase with increasing deposition time. For the films annealed at different annealing temperatures, all films are found to have a columnar structure perpendicular to the surface with uniform distribution of spherical grains, as shown in Fig. 6. This can be understood that as the temperature increases, atoms gain more energy to migrate and have enhanced mobility, which contributes to the formation of uniform grains to a certain degree.

Figure 7 provides V(z) curves of ZnO thin films deposited for various hours. With increasing deposition time, Δz values decrease while not much difference in peak heights is observed among various deposition time conditions. The level of high frequency noise becomes severe for thicker films particularly when z is in the range of −250 μm to 100 μm. In Fig. 8, a plot of LSAW velocities determined from V(z) curves generated at 400 MHz excitation frequency with different ZnO film thickness. It is apparent that LSAW velocity strongly depends on film thickness, which is expected as SAW dispersion properties in thin film structures. The phase velocity of LSAWs monotonically decreases from 5328.3 m/s and asymptotically approaches to 4245.7 m/s with film thickness increasing from 32.5 nm to 2.04 μm. This can be explained by the distribution of the transmitted acoustic energy between film and substrate. Since the acoustic wave can penetrate relatively deeper into the substrate in a thinner film, most of the transmitted acoustic energy is localized in the substrate and thus, the phase velocity of the LSAW approaches the Rayleigh velocity of the substrate material [36, 37]. As film thickness increases, more energy is localized inside the ZnO film layer and therefore, the LSAW velocity approaches the Rayleigh velocity of the bulk ZnO. The Rayleigh velocity of Si is higher than that of ZnO and therefore, LSAW tends to decrease with increasing ZnO film thicknesses, as observed in Fig. 8. The decreasing dependence of LSAW velocities on film thickness in Fig. 8 can also be explained by acoustoelasticity. According to acoustoelasticity, compressive residual stresses normally increase the acoustic velocity. Hence, relaxation of compressive residual stress decreases the acoustic velocity, so does LSAW velocity with increasing film thicknesses in Fig. 8.

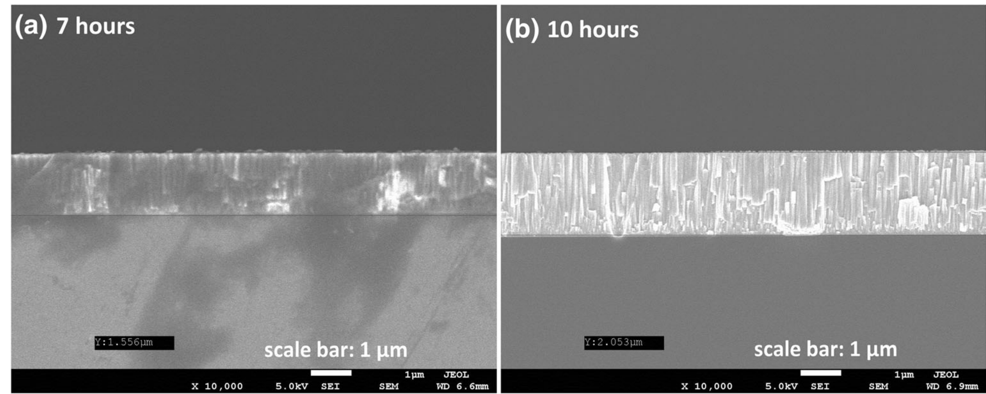

Fig. 5 Cross-section SEM images of the ZnO films deposited for (**a**) 7 h and (**b**) 10 h

Du et al. previously reported dispersive properties of SAW velocities of ZnO films deposited on Si (100) in [37]. In their work, SAW velocities decrease from 4352 m/s to 3456 m/s while film thickness increases from 1.5 μm to 6.6 μm. Although the propagation mechanism of LSAW is slightly different from that of SAW, the magnitude and the dispersive trends in the LSAW velocities obtained in this work and the previously reported SAW velocities are found similar, which proved useful to check the validity.

In Fig. 8, even a slight increase from 4146.0 m/s to 4245.7 m/s occurs in the LSAW velocities when film thickness varies from 1.47 μm to 2.04 μm. These two thicknesses are the results from film deposition for 7 h and 10 h, respectively. This is in distinct contrast with the theoretical prediction that much further decrease rather than a slight increase would appear for thicker films until it reaches the Rayleigh velocity of bulk ZnO, which is known to be 2700 m/s [38]. Two possible mechanisms can be addressed for this phenomenon. First, it might be related to the degree of orientation and crystallinity. Both XRD analysis and SEM images confirmed that ZnO films sputtered for 7 and 10 h exhibit distinct columnar structures and better preferred orientation. In [39], Liaw and Hickernell presented that better orientation of AlN grains might be attributed to higher SAW phase velocity in AlN film on [100] Si substrates. The authors of [39] plotted the change in the SAW velocity as a function of the ratio of AlN thickness to acoustic wavelength and compared their experimental dispersion curves with a theoretical curve derived by Tsubouchi and

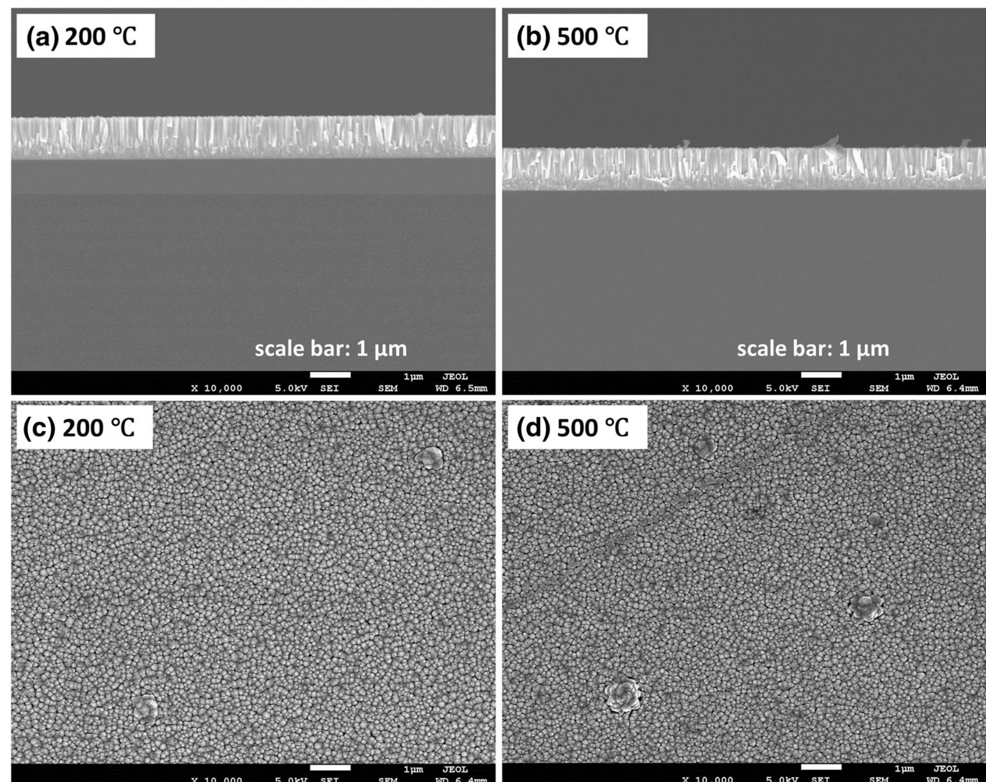

Fig. 6 Cross-section SEM images and plan-views of the ZnO films annealed at (**a**), (**c**) 200 °C and (**b**), (**d**) 500 °C, respectively

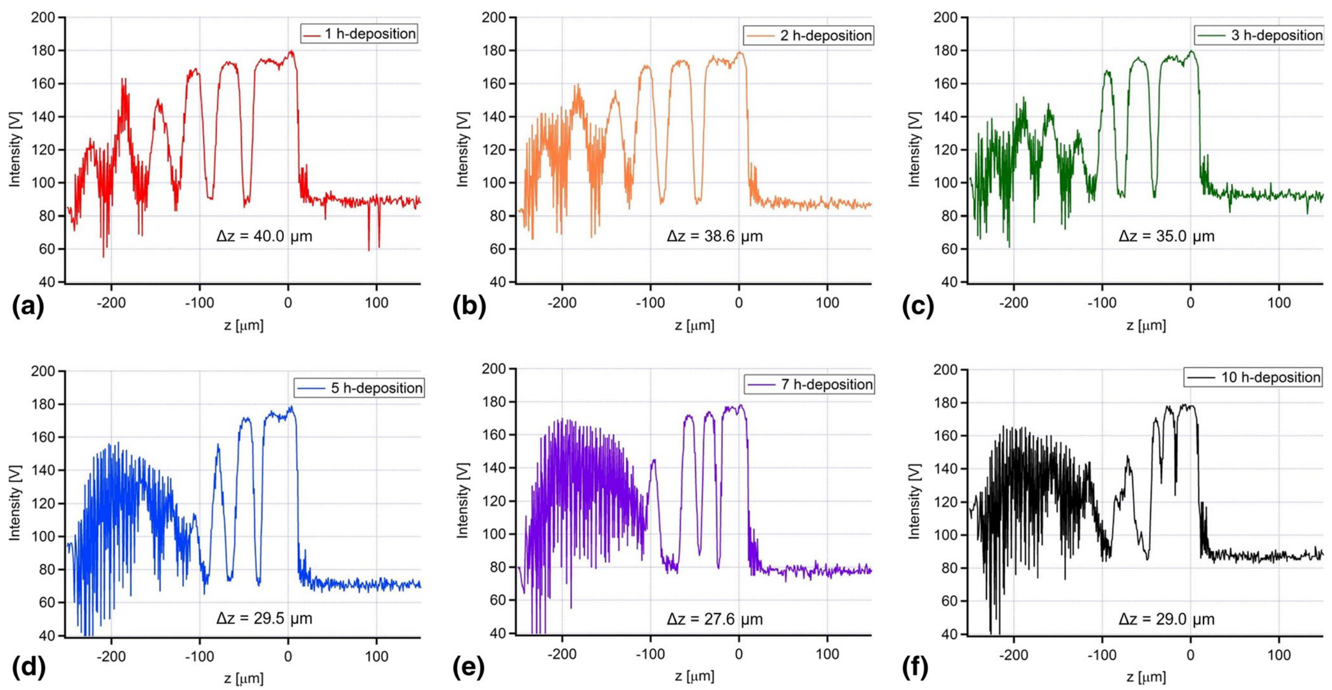

Fig. 7 V(z) curves of the ZnO films deposited for (**a**) 1 h, (**b**) 2 h, (**c**) 3 h, (**d**) 5 h, (**e**) 7 h, (**f**) 10 h

Mikoshiba in [40]. The theoretical dispersion from Tsubouchi model suggested that the SAW velocity increases from the minimum due to the higher elasticity associated with the better orientation. The slight increase in the LSAW velocity observed in Fig. 8 also seem to confirm the argument made by the authors of [39, 40]. Second, the increased LSAW velocity locally observed might be related to the surface roughness. To investigate the effect of surface roughness on LSAW velocities, the results of the AFM measurements are depicted in Figs. 8 and 9. As deposition time increases, film thickness increases. Meanwhile, roughness gets increased to a certain point and then drops to very low values for thicker films that

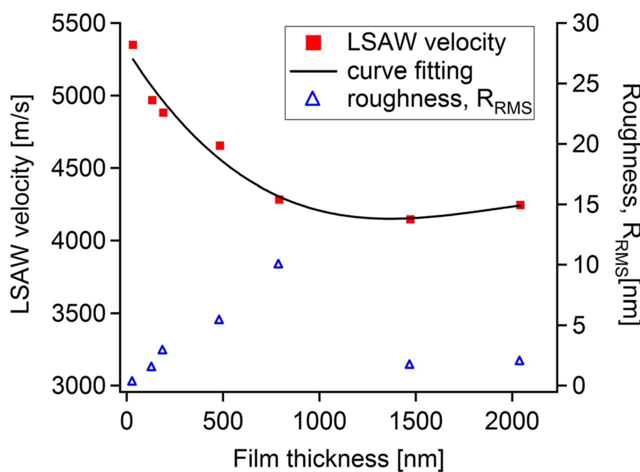

Fig. 8 LSAW velocities and RMS roughness (R_{RMS}) as a function of film thickness

were deposited for 7 and 10 h. Long deposition time sufficient for the grain growth seems to contribute to the formation of smoother surface. Acoustic waves can propagate much faster on smoother surface rather than rough surface. According to Liaw and Hickernell [39], films with smaller grain sizes are likely to exhibit smoother surface, which is attributed to the higher elasticity associated with the improvement in the preferred orientation. Similar to the case of AlN on Si in [39], the change in the LSAW velocity in this work also has dependence on the surface roughness via the improvement in the orientation (hence the increase in the elastic constant). Thickness dependence leads to the decrease of LSAW velocity while smooth surface results in the increase of LSAW velocity. Combination of both effects of thickness and surface conditions might be the results of LSAW velocities at thicknesses of 1.47 μm and 2.04 μm in the plot of Fig. 8.

The influence of annealing temperature on the LSAW velocities and surface roughness is also investigated. As mentioned previously, there is little variation in the thickness of ZnO films annealed at various temperatures, which is demonstrated in Fig. 10. Accordingly, not much difference appears among the LSAW velocities of these films. The values of LSAW velocities seem slightly distinctive from the rest in the plot of Fig. 10 when the annealing temperature corresponds to 550 °C and 600 °C. At these conditions, the expected behavior would be faster speed according to SAW dispersion effect since film thickness gets decreased slightly. On the contrary, LSAW velocities are decreased, which might be due to the relaxation of the compressive residual stress. According to acoustoelasticity, compressive residual stresses increase the

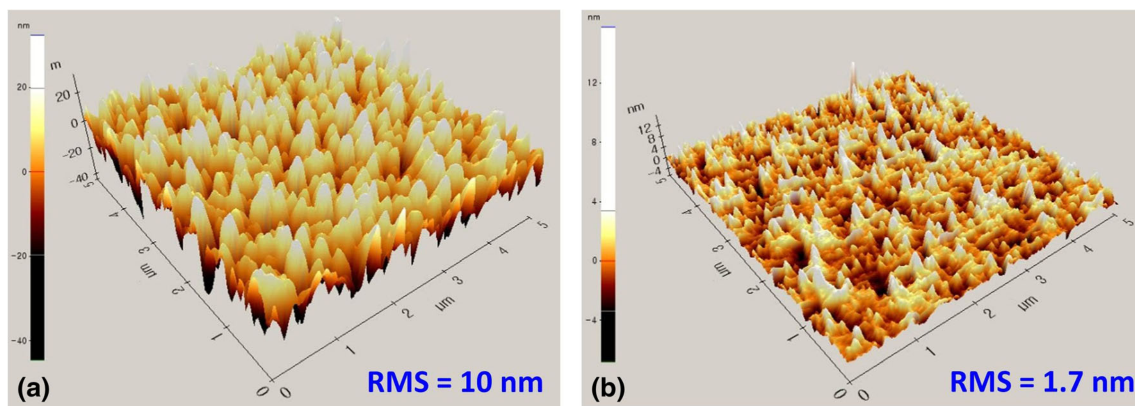

Fig. 9 Three-dimensional AFM images and RMS values of surface roughness for ZnO films deposited for (**a**) 5 h and (**b**) 7 h

acoustic wave velocity. If a compressive residual stress is relaxed by annealing at high temperature such as 550 °C and 600 °C, it is possible that the LSAW velocity decreases.

4 Conclusions

Highly crystalline ZnO thin films were deposited and characterized to investigate the structural and acoustic properties as a function of sputtering conditions. The correlation of surface acoustic properties of ZnO thin films with thin film growth was thoroughly studied through X-ray diffraction, atomic force microscopy, scanning electron microscopy, and scanning acoustic microscopy techniques. In particular, scanning acoustic microscopy provided a useful method to determine the velocities of surface acoustic waves of ZnO thin film without a need for additional device fabrication with electrodes. It was found that surface acoustic wave propagation in ZnO thin films was closely related to film thickness, crystallinity, grain structure, and surface roughness. The velocities of LSAW had a distinct dispersion to film thickness and decreased from 5328.3 m/s to 4245.7 m/s with increasing film thickness from 32.5 nm to 2.04 μm. Additionally, higher crystallinity and smoother surface seemed to result in faster acoustic propagation. These results will help understanding the behavior of acoustic wave propagation in ZnO thin films as well as provide useful information on the magnitude of SAW velocities in ZnO thin films as a function of sputtering conditions.

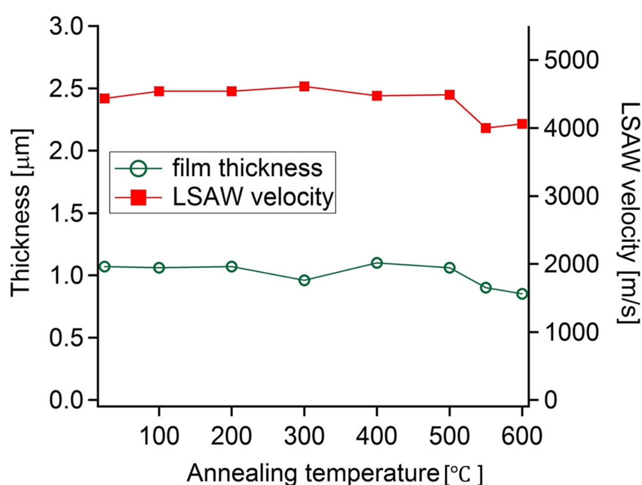

Fig. 10 Thickness and LSAW velocity of the ZnO films annealed at various temperatures

Acknowledgements This work was supported by the National Research Foundation of Korea funded by the Ministry of Science, ICT & Future Planning (NRF-2013M2A2A9043274).

References

1. X.L. Zhang, K.N. Hui, K.S. Hui, J. Singh, Mater. Res. Bull. **48**, 1093 (2013)
2. A.M. Rosa, E.P. da Silva, M. Chaves, L.D. Trino, P.L. Lisboa-Filho, T.F. da Silva, S.F. Durrant, J.R.R. Bortoleto, J. Mater. Sci. – Mater. Electron **24**, 3143 (2013)
3. Y.M. Lu, W.S. Hwang, W.Y. Liu, J.S. Yang, Mater. Chem. Phys. **72**, 269 (2001)
4. M.-Y. Han, J.-H. Jou, Thin Solid Films **58**, 58 (1995)
5. J. Hinze, K. Ellmer, J. Appl. Phys. **88**, 2443 (2000)
6. S.-Y. Chu, W. Water, J.-T. Liaw, J. Eur. Ceram. Soc. **23**, 1593 (2003)
7. W. Water, S.-Y. Chu, Mater. Lett. **55**, 67 (2002)
8. K.A. Sierros, D.A. Banerjee, N.J. Morris, D.R. Cairns, I. Kortidis, G. Kiriakidis, Thin Solid Films **519**, 325 (2010)
9. Z. Yu, S. Boseck, RMP **67**, 863 (1995)
10. S.S. Lee, B. Ahn, K. Yamanaka, J. Mater. Sci. **34**, 6095 (1999)
11. R.A. Lemons, C.F. Quate, *Acoustic microscopy* (ACADEMIC PRESS Inc., New York, 1979), pp. 2–90
12. A. Atalar, J. Appl. Phys. **49**, 5130 (1978)
13. R.D. Weglein, Appl. Phys. Lett. **34**, 179 (1979)
14. D.E. Chimenti, A.H. Nayfeh, D.L. Butler, J. Appl. Phys. **53**, 170 (1982)
15. A.G. Every, M. Deschamps, Ultrasonics **41**, 581 (2003)
16. A. Habib, A. Shelke, M. Vogel, U. Pietsch, X. Jiang, T. Kundu, Ultrasonics **52**, 989 (2012)

17. L. Robert, N. Brunet, T. Flaherty, T. Randles, E. Matthaei-Schulz, H. Vetters, D. Rats, J. von Stebut, Surf. Coat. Technol. **116**, 327 (1999)
18. R.D. Weglein, IEEE Trans. Sonics. Ultrason. **27**, 82 (1980)
19. T. Kundu, A.K. Mal, R.D. Weglein, J. Acoust. Soc. Ame. **77**, 353 (1985)
20. J.D. Achenbach, J.O. Kim, Y.-C. Lee, in Advances in acoustic microscopy, ed. By A. Briggs (Springer, New York, 1995), pp. 153–208
21. W. Li, J.D. Achenbach, IEEE Ultrason. Symp. **2**, 883 (1995)
22. M.J. Bamber, K.E. Cooke, A.B. Mann, B. Derby, Thin Solid Films **398**, 299 (2001)
23. A. Benbelghit, D. Boutassouna, B. Helifa, I.K. Lefkaier, NDT. E. Int. **39**, 76 (2006)
24. J. Du, B.R. Tittmann, H.S. Ju, Thin Solid Films **518**, 5786 (2010)
25. J. Albertsson, S.C. Abrahams, Å. Kvick, Acta Crystallographica Section B: Structural **45**, 34 (1989)
26. G.S. Pawley, J. Appl. Crystallogr. **14**, 357 (1981)
27. N. Panwar, J. Liriano, R.S. Katiyar, J. Alloys Compd. **509**, 1222 (2011)
28. D.D.A. Santos, A.D.P. Rocha, M.A. Macedo, Powder Diffract. **23**, S36 (2008)
29. H. Karzel, W. Potzel, M. Kofferlein, W. Schiessl, M. Steiner, U. Hiller, G.M. Kalvius, D.W. Mitchell, T.P. Das, P. Blaha, K. Schwarz, M.P. Pasternak, Phys. Rev. B **53**, 11425 (1996)
30. H. Schulz, K.H. Thiemann, Solid State Commun. **32**, 783 (1979)
31. O. Garcia-Martinez, R.M. Rojas, E. Vila, J.M. De Vidales, Solid State Ionics **63**, 442 (1993)
32. R. Escudero, R. Escamilla, Solid State Commun. **151**, 97 (2011)
33. R. Hong, J. Huang, H. He, Z. Fan, J. Shao, Appl. Surf. Sci. **242**, 346 (2005)
34. A.L. Patterson, Phys. Rev. **56**, 978 (1939)
35. M.H. Weng, C.T. Pan, R.Y. Yang, C.C. Huang, Ceram. Int. **37**, 3077 (2011)
36. A. Talbi, F. Sarry, L. Le Brizoual, O. Elmazria, P. Alnot, IEEE Trans. Ultrason. Ferroelect. Freq. Contr. **51**, 1421 (2004)
37. X.Y. Du, Y.Q. Fu, S.C. Tan, J.K. Luo, A.J. Flewitt, W.I. Milne, D.S. Lee, N.M. Park, J. Park, Y.J. Choi, S.H. Kim, S. Maeng, Appl. Phys. Lett. **93**, 094105 (2008)
38. V. Panella, G. Carlotti, G. Socino, L. Giovannini, M. Eddrief, K. Amimer, C. Sebenne, J. Phys. Condens. Matter **9**, 5575 (1997)
39. H.M. Liaw, F.S. Hickernell, IEEE Trans. Ultrason. Ferroelect. Freq. Contr. **42**, 404 (1995)
40. K. Tsubouchi, N. Mikoshiba, IEEE Trans. Son. and Ultrason. **32**, 634 (1985)